



Dual PIO-Based Controller Design for Robustness Improvement of a Magnetic Levitation System

Nebiyeleul Daniel Amare¹ · Young Ik Son¹ · Seungchul Lim²

Received: 19 October 2019 / Revised: 3 January 2020 / Accepted: 20 February 2020 / Published online: 13 March 2020
© The Korean Institute of Electrical Engineers 2020

Abstract

Magnetic levitation systems have a high potential in industrial applications. However, their nonlinear and open-loop unstable nature combined with susceptibility to system parameter uncertainties and external disturbances poses a challenging control problem. As a result, most control techniques applied to these systems are advanced but complex. This paper proposes a proportional–integral observer (PIO)-based control scheme still using a simple conventional cascade controller to enhance robustness. Design of the controller is presented along with computer simulations to verify that the controller is capable of maintaining nominal performance even under such severe conditions. In addition, the performance of the observer’s compensatory action is analyzed according to the singular perturbation theory.

Keywords Magnetic levitation system · Robust control · Proportional–integral observer (PIO) · Cascade configuration control · Singular perturbation theory

1 Introduction

Magnetic levitation, also referred to as maglev, is an art by which a ferromagnetic object is levitated or suspended at a desired position using an electromagnet without any mechanical support. Such a method offers numerous advantages such as the elimination of lubrication systems and lowered rotating losses, providing higher speed and long-life services [1]. Due to those, maglev systems have found

applications in many sophisticated areas including aircraft launch systems [2], maglev trains [3], nanoscale positioning systems [4], and vibration isolation of sensitive devices [5].

However, maglev systems have an unstable equilibrium point and nonlinear dynamic structures, which makes them challenging from a control point of view [5]. In addition, just like any other systems, they are susceptible to parameter uncertainties and external disturbances. This makes preserving the nominal performance of maglev systems with conventional controllers impossible under such severe conditions. As a result, maglev system has attracted a lot of attention from control society [5–13], and a variety of techniques have been proposed with the desire to achieve and maintain nominal performance. Among them are internal model-based robust regulator [6], adaptive robust control by K-filter approach [7], robust position estimation based on least square identification [8], nonlinear model predictive control [9], 2-DOF PID controller [10], neural-network-based control [11], sliding mode control [12], active disturbance rejection control [13], etc. The majority of those and other methods reported so far are advanced.

But despite all the advanced methods available, the conventional cascade configuration is worth reconsidering as a basic scheme owing to its practicality and ability to be decoupled during design for nominal performance. Also, cascade control structure is one of the most common control

This work was supported by the National Research Foundation of Korea (NRF) Grant funded by the Korea government (MSIT) (No. 2019R1F1A1058543). This research was supported by Korea Electric Power Corporation (Grant Number: R17XA05-2).

✉ Young Ik Son
sonyi@mju.ac.kr

Nebiyeleul Daniel Amare
nebiyeleul1@gmail.com

Seungchul Lim
slim@mju.ac.kr

¹ Department of Electrical Engineering, Myongji University, 116 Myongji-ro, Cheoin-gu, Yongin-si, Gyeonggi-do 17058, South Korea

² Department of Mechanical Engineering, Myongji University, 116 Myongji-ro, Cheoin-gu, Yongin-si, Gyeonggi-do 17058, South Korea

strategies in industrial processes to dramatically improve the performance of single-loop control, reducing both the maximum deviation and the integrated error of the disturbance response [14].

The controller that is commonly used in cascade configuration is proportional–integral (PI). Compared to other kinds, it is more suitable for practical implementation. And its main advantage is the ability to ensure zero steady-state error under low-frequency disturbances and model uncertainties as long as the closed-loop system is stable. However, the transient performance of PI controller depends on the system parameters, external disturbance, and input constraints [15]. Hence, this controller might be regarded as feasible but not robust enough.

Due to its practical importance, the design of a robust controller for systems affected by system parameter uncertainties and unmeasurable external disturbances has also been an area of active research. Therefore various approaches have been also proposed [16]. One well-known strategy is based on estimation and compensation, wherein effect of uncertainties and disturbances on the system is estimated and compensated by augmenting the controller designed for a nominal system [17–25]. The design procedure of such a disturbance observer-based controller has two stages. The first one focuses on stabilizing the plant performance under nominal conditions, while the other is about designing a disturbance observer (DOB) to compensate for the disturbance effects. Then, the designed DOB is integrated with the controller.

Motivated by Beale and Shafai [26] and Kim and Son [27], this paper proposes an approach in which a conventional cascade configuration controller, which can maintain nominal performance basically in the absence of system parameter uncertainty and external disturbance, is to be modified: by integrating it with two proportional–integral observers (PIOs) the system can maintain nominal performance even in their presence. The novelty of the method lies not in the use of PIO (or DOB) but in the use of dual PIOs for a nonlinear maglev system. In various cases, the proposed method has outperformed the ones that employed a single PIO [26]. Since the proposed controller suggests enhancement of robustness by modifying an already existing controller, it can be said that the advantage of the proposed control scheme is its ability to eliminate the need to design a new controller.

A theoretical analysis is also performed on such augmented system to illustrate the performance recovery property of the PIO from system uncertainties. The key tool used in that course is the singular perturbation theory [28], which arises from the fast PIO dynamics. A stability condition for the fast boundary-layer system is found out to determine observer gains such that the real uncertain system recovers the nominal plant without uncertainties. While the stability

condition depends on a real system parameter, it can be made Hurwitz by adjusting the observer parameters. Under the condition, it is shown that the quasi-steady-state system closely approximates the nominal plant as the observer poles are placed sufficiently left of the complex s -plane.

This paper's contributions may be summarized as follows:

1. A new cascade control approach is presented for a single-axis magnetic levitation system by combining a PI–PI cascade control and two nested PIOs to maintain desirable performance of the conventional closed-loop system even in the presence of uncertainties and disturbances.
2. Theoretical analysis is carried out on the performance of the closed-loop magnetic levitation system with the PIO, which confirms the desired approximation of the augmented system to the conventional closed-loop system without uncertainties.
3. Comparative computer simulations are conducted to verify the theoretical analysis.

The rest of the paper is organized as follows. Section 2 introduces the maglev system under consideration and its mathematical model. And subsequently, the conventional cascade controller design is presented along with a simulation result to study its performance under the influence of parameter uncertainty and disturbances. Based on the simulation, its weakness and the way it can be corrected are discussed. In Sect. 3 a PIO is briefed, and the proposed controller is designed. After the design, the robustness of the observer is analyzed in Sect. 4 using the singular perturbation theory. In Sect. 5 significant simulation results are presented verifying the performance of the proposed controller. In particular, the performances of various versions of the proposed controller are compared. Finally the next section concludes the paper.

2 System Model and Conventional Control Scheme

2.1 System Model

The basic principle of a magnetic levitation system operation is to apply a voltage to an electromagnet to generate sufficient magnetic force to keep a ferromagnetic object levitated. The magnetic levitation system considered here is a single-axis system (Fig. 1). That is, the ball can only move in the vertical direction. The current of the overhead electromagnet can be adjusted either to make the ball stay at a given position or to drive the ball to track a desired trajectory [12, 13].

The equations describing the motion of the ferromagnetic ball and the current of the electric circuit are respectively

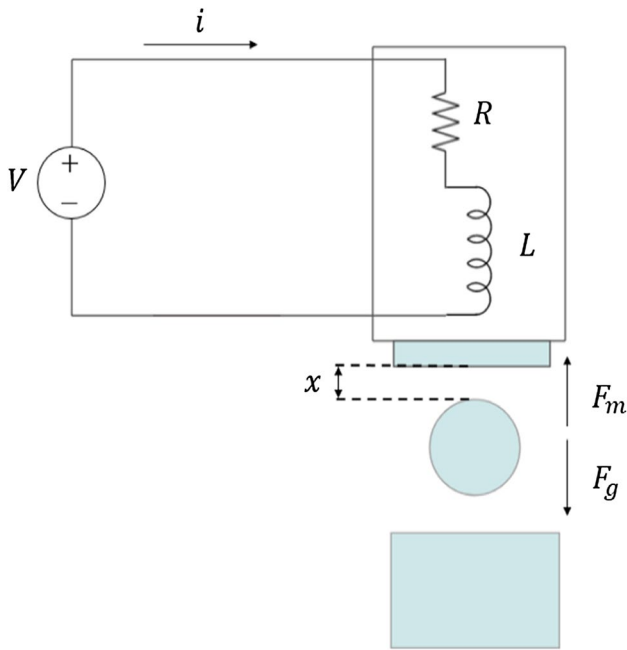


Fig. 1 Schematic diagram of the maglev system

$$\ddot{x} = g - \frac{G_i}{m} \left(\frac{i}{x} \right)^2, \tag{1a}$$

$$L \frac{di}{dt} = -Ri + V \tag{1b}$$

where x represents the air gap or equivalently the ball’s position, i is the current passing through the electromagnet, m is the ball mass, g is the gravitational acceleration, G_i denotes the magnetic force constant for the electromagnet/ball pair at hand, R is the total resistance of the circuit, and L is the coil inductance. The $G_i(i/x)^2$ term in (1a) characterizes the nonlinear relationship among the magnetic force, the current, and the ball position [12].

According to (1a), if the gravitational force (F_g) and the magnetic force (F_m) acting on the ball balance, then $\ddot{x} = 0$. Thus the current that can bring such a steady state is

$$i_e = x_e \sqrt{\frac{gm}{G_i}} \tag{2}$$

where x_e is the desired constant position and i_e is the corresponding current.

Theoretically, it is possible to achieve steady levitation of the ball by continuously providing the electromagnet with i_e . But this cannot be guaranteed due to the open-loop unstable nature of the magnetic levitation system [13]. Therefore, to keep the ball in a steady state, a real-time closed-loop controller is required so that the two forces can always cancel out.

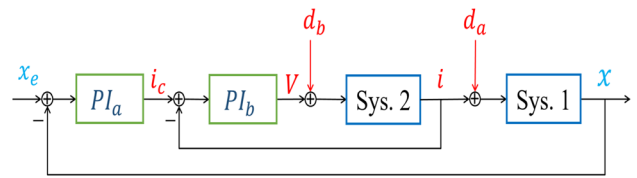


Fig. 2 PI-PI cascade configuration controller, where d_a and d_b stand for the equivalent disturbances in the outer and inner-loop system respectively

2.2 Conventional Control Scheme

One of the most popular control schemes applied to systems concatenated as in (1), consists of multiple controllers in a cascade configuration [29]. By treating the electromechanical system (1a) and the electrical system (1b) as separate subsystems, one can design two individual controllers. Equation (1a) will be used to design a ball position controller in the outer loop that tracks a desired reference ball position. That controller produces the reference current to be tracked by the inner-loop controller which amounts to the current controller. (The electromechanical and the electrical subsystem are labeled as Sys. 1 and Sys. 2 respectively in Figs. 2 and 5. Likewise, throughout the paper the subscript a is used to represent outer-loop equations and components, while the subscript b inner-loop counterparts.)

In order to design the outer-loop controller, (1a) needs to be linearized at point (x_e, i_e) to yield

$$\ddot{x} = \frac{2G_i i_e^2}{x_e^3 m} x - \frac{2G_i i_e}{x_e^2 m} i \tag{3a}$$

$$\triangleq a_M x - b_M i. \tag{3b}$$

Once the linearized equation is obtained, a state feedback controller is designed using the state space representation

$$\begin{bmatrix} \dot{\xi}_1 \\ \dot{\xi}_2 \\ \dot{\zeta}_x \end{bmatrix} = \begin{bmatrix} 0 & 1 & 0 \\ a_M & 0 & 0 \\ 1 & 0 & 0 \end{bmatrix} \begin{bmatrix} \xi_1 \\ \xi_2 \\ \zeta_x \end{bmatrix} + \begin{bmatrix} 0 \\ -b_M \\ 0 \end{bmatrix} i. \tag{4}$$

where $\xi_1 = x$, $\xi_2 = \dot{x}$, and ζ_x is the extra state variable used to calculate the I gain. The reference current provided by the outer-loop controller is given

$$i_c = -k_{p1}(\xi_1 - x_e) - k_{p2}\xi_2 - k_{I1} \int_0^t (\xi_1 - x_e) d\tau \tag{5}$$

where k_{p1} , k_{p2} and k_{I1} are the controller gains.

For the subsystem (1b) the inner-loop controller is designed using the corresponding state equation

$$\begin{bmatrix} \dot{\xi}_3 \\ \dot{\zeta}_i \end{bmatrix} = \begin{bmatrix} -R/L & 0 \\ 1 & 0 \end{bmatrix} \begin{bmatrix} \xi_3 \\ \zeta_i \end{bmatrix} + \begin{bmatrix} 1/L \\ 0 \end{bmatrix} V \tag{6}$$

where the state $\xi_3 = i$, and ζ_i is the state variable serving same purpose as ζ_x above. Then, the inner-loop controller is to supply the control input

$$V = -k_{p3}(\xi_3 - i_c) - k_{i2} \int_0^t (\xi_3 - i_c) d\tau. \tag{7}$$

2.3 Limitations of Conventional Controller

The performance of the conventional controller has been analyzed through a computer simulation. The simulation tests and shows the controller’s performance under four conditions in Fig. 3: nominal (the green line), with system parameter uncertainties (the blue dotted line), with the influence of external disturbance (the red dashed line), and with the uncertainty and disturbance combined (the black line). Those conditions are more detailed in Sect. 5.

From Fig. 3 it can be seen that the conventional controller solely maintains nominal performance in the circumstance free from system parameter uncertainties and external disturbance. The presence of system parameter uncertainty degrades the transient-state response of the system, while that of external disturbance disrupts the system’s steady-state performance. Also, the controller fails to regain nominal performance when the external disturbance takes a form of a time-varying function. Hence, the conventional controller is not considered robust enough.

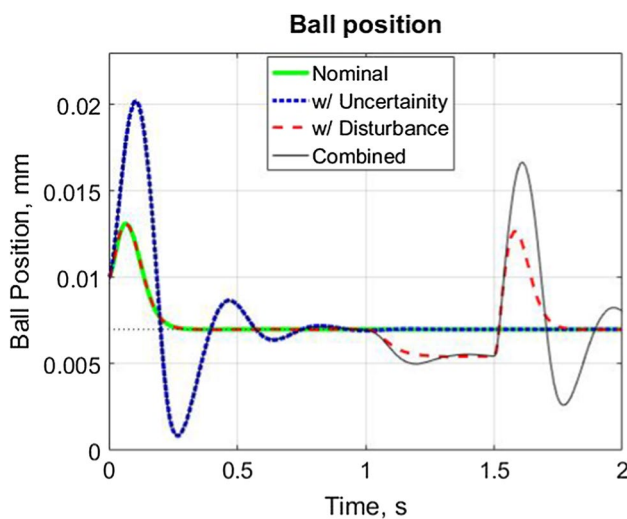


Fig. 3 Simulation result illustrating the performance degradation of the PI-PI cascade configuration controller due to system parameter uncertainty and time-varying disturbance

3 Robust Performance via PIO-Based Controller

In this section, a proportional–integral observer is briefly introduced and then two individual PIOs will be designed for both control loops mentioned in the previous section.

3.1 Proportional–Integral Observer (PIO)

A PIO is a type of disturbance observer (DOB). The primary role of DOBs is to compensate an uncertain system affected by disturbance so that the controller designed, just for the nominal disturbance-free model of the plant, recovers robust stability and performance [18, 20, 21]. PIO uses two feedback loops to reconstruct system states and the equivalent disturbance which is a combination of the effects of unknown inputs, system parameter uncertainties and unmodeled system dynamics or modeling errors. Once the equivalent disturbance is estimated, it is subtracted from the original control input to cancel out the undesired influence (as can be seen in Fig. 4). Therefore, important is to find \hat{d} , the equivalent disturbance estimate.

The state-space model of an n th order, p input, q output plant with p independent disturbances of constant value can be represented by

$$\dot{x} = Ax + B(u + d), \quad y = Cx, \tag{8a}$$

$$\dot{d} = 0. \tag{8b}$$

The equations above can be put together defining a new state vector $z = [x^T, d^T]^T$. Thus, the augmented model of the plant can be written

$$\dot{z} = \begin{bmatrix} A & B \\ 0 & 0 \end{bmatrix} \begin{bmatrix} x \\ d \end{bmatrix} + \begin{bmatrix} B \\ 0 \end{bmatrix} u \triangleq A_z z + B_z u \tag{9a}$$

$$y = [C \quad 0] \begin{bmatrix} x \\ d \end{bmatrix} \triangleq C_z z. \tag{9b}$$

Now a PIO is designed as below.

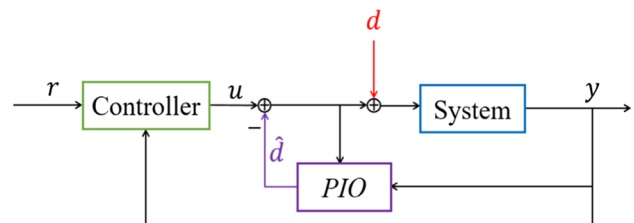


Fig. 4 Controller with a PIO, where r is the reference signal, u is the control input, d is external disturbance, and y is the system output

$$\dot{\hat{z}} = A_z \hat{z} + B_z u + L_z (C_z z - C_z \hat{z}) \tag{10}$$

where $L_z = [L_p^T \ L_I^T]^T$. Then the dynamics of the estimation error turns out

$$\dot{e}_z \triangleq \dot{z} - \dot{\hat{z}} = (A_z - L_z C_z) e_z. \tag{11}$$

Thus, as long as the matrix $A_z - L_z C_z = \begin{bmatrix} A - L_p C & B \\ -L_I C & 0 \end{bmatrix}$ is Hurwitz, the error between actual and estimated state variables will decay to zero as time goes to infinity.

3.2 Dual PIO-Based Controller

To maintain its advantage, this paper employs a control structure composed of two PI controllers in a conventional cascade configuration. Instead, two PIOs are supplemented to the control loops to enhance robustness. With their assistance, the controller proposed, as can be seen in Fig. 5, takes the effect of the disturbance into consideration and counteracts its undesired influence.

The PIO_a for the outer loop is designed for the subsystem (3). So, following (10) its model is

$$\dot{\hat{z}}_a = A_a \hat{z}_a + B_a i + L_a (C_a z_a - C_a \hat{z}_a) \tag{12}$$

where $z_a = [z_1 \ z_2 \ d_a]^T = [x \ \dot{x} \ d_a]^T$, and coefficient matrices A_a, B_a, C_a and L_a are

$$A_a = \begin{bmatrix} 0 & 1 & 0 \\ a_M & 0 & -b_M \\ 0 & 0 & 0 \end{bmatrix}, B_a = \begin{bmatrix} 0 \\ -b_M \\ 0 \end{bmatrix}, C_a = \begin{bmatrix} 1 & 0 & 0 \\ 0 & 1 & 0 \end{bmatrix}, L_a = \begin{bmatrix} l_{11} & l_{21} & l_{31} \\ l_{12} & l_{22} & l_{32} \end{bmatrix}^T.$$

The PIO_a is to estimate the ball’s position (x) and velocity (\dot{x}). It additionally does the equivalent disturbance present in the subsystem \hat{d}_a . Using these estimates the reference current is set to

$$i_r = i^* - \hat{d}_a \tag{13}$$

where $i^* = -k_{p1} \bar{z}_1 - k_{p2} \bar{z}_2 - k_{I1} \int_0^t \bar{z}_1 d\tau$ with $\bar{z}_1 = \hat{z}_1 - x_e$ like (5). Therefore, the reference current i_r , modified by the proposed controller is obtained by subtracting the estimated equivalent disturbance, \hat{d}_a , from the original reference current i^* .

Meanwhile, the inner-loop observer is designed through the same procedure. For the electrical subsystem (1b), the model of PIO_b is

$$\dot{\hat{z}}_b = A_b \hat{z}_b + B_b V + L_b (C_b z_b - C_b \hat{z}_b) \tag{14}$$

where $z_b = [z_3 \ d_b]^T = [i \ d_b]^T$, L_b is the observer gain matrix, and the remaining matrices are

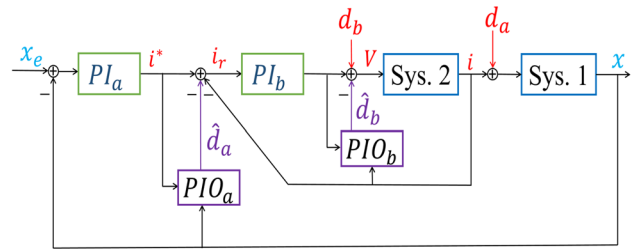


Fig. 5 Controllers with two PIOs in cascade configuration, where \hat{d}_a and \hat{d}_b represent the equivalent disturbance estimates in their respective loops

$$A_b = \begin{bmatrix} -R/L & 1/L \\ 0 & 0 \end{bmatrix}, B_b = \begin{bmatrix} 1/L \\ 0 \end{bmatrix}, C_b = [1 \ 0]. \tag{15}$$

Obviously, PIO_b estimates the current denoted by z_3 and the disturbance d_b . Consequently the control input, which is the output of the inner-loop controller, becomes

$$V = -k_{p3} (\hat{z}_3 - i_r) - k_{I2} \int_0^t (\hat{z}_3 - i_r) d\tau - \hat{d}_b. \tag{16}$$

4 Theoretical Performance Analysis

In here, the performance of the feedforward compensation by PIO_a is analyzed according to the singular perturbation theory [28]. The \hat{d}_a is the estimation of d_a , which represents the combined effect of the external disturbance and the system uncertainties in the outer loop. When $i = i_r = i^* - \hat{d}_a$, the outer-loop system is governed by

$$\dot{x}_1 = x_2 \tag{17a}$$

$$\dot{x}_2 = a_M x_1 - b_M (i^* - \hat{d}_a + d). \tag{17b}$$

If the model of PIO_a in (12) is written out, it appears

$$\dot{\hat{x}}_1 = \hat{x}_2 + l_{11} \tilde{x}_1 + l_{12} \tilde{x}_2 \tag{18a}$$

$$\dot{\hat{x}}_2 = \hat{a}_M \hat{x}_1 - \hat{b}_M i^* + l_{21} \tilde{x}_1 + l_{22} \tilde{x}_2 \tag{18b}$$

$$\dot{\hat{d}}_a = l_{31} \tilde{x}_1 + l_{32} \tilde{x}_2 \tag{18c}$$

where $\tilde{x}_i = x_i - \hat{x}_i$ ($i = 1, 2$), \hat{a}_M and \hat{b}_M are the nominal values of a_M and b_M respectively, unaltered by system parameter uncertainty.

When $a_M = \hat{a}_M, b_M = \hat{b}_M$, and $d = d_a$, the observer error dynamics in (11) leads to

$$\begin{bmatrix} \dot{\tilde{x}}_1 \\ \dot{\tilde{x}}_2 \\ \dot{\tilde{d}}_a \end{bmatrix} = \begin{bmatrix} -l_{11} & -(l_{12} - 1) & 0 \\ -(l_{21} - \hat{a}_M) & -l_{22} & -\hat{b}_M \\ -l_{31} & -l_{32} & 0 \end{bmatrix} \begin{bmatrix} \tilde{x}_1 \\ \tilde{x}_2 \\ \tilde{d}_a \end{bmatrix} \quad (19)$$

where $\tilde{d}_a = d_a - \hat{d}_a$. By using the observer gain

$$L_a = \begin{bmatrix} k_1/\epsilon & \hat{a}_M & 0 \\ 1 & k_2/\epsilon & -k_3/(\hat{b}_M \epsilon^2) \end{bmatrix}^T, \quad (20)$$

one can obtain the characteristic equation of (19) as follows:

$$\left(s + \frac{k_1}{\epsilon}\right) \left(s^2 + \frac{k_2}{\epsilon}s + \frac{k_3}{\epsilon^2}\right) = 0. \quad (21)$$

Therefore, if $\epsilon > 0$ and $k_i > 0$ ($i = 1, 2, 3$), (21) is Hurwitz. When $k_1 = k_3 = 1$ and $k_2 = 2$, for example, three roots are located all at $s = -1/\epsilon$.

On the other hand, when $\hat{a}_M \neq a_M, \hat{b}_M \neq b_M$ and $d_a \neq d$, the observer error dynamics changes to

$$\dot{\tilde{x}}_1 = -\frac{k_1}{\epsilon} \tilde{x}_1 \quad (22a)$$

$$\dot{\tilde{x}}_2 = -\frac{k_2}{\epsilon} \tilde{x}_2 + b_M \hat{d}_a + \delta \quad (22b)$$

$$\dot{\tilde{d}}_a = -\frac{1}{\hat{b}_m} \frac{k_3}{\epsilon^2} \tilde{x}_2 \quad (22c)$$

where $\delta = (a_M - \hat{a}_M)x_1 - b_M d - (b_M - \hat{b}_M)i^*$.

Introducing a pair of new state variables

$$\eta_1 = \frac{1}{\epsilon} \tilde{x}_1, \quad \eta_2 = \frac{1}{\epsilon} \tilde{x}_2, \quad (23)$$

(17) and (22) can be put into the standard singular perturbation form;

$$\dot{x}_1 = x_2 \quad (24a)$$

$$\dot{x}_2 = a_M x_1 - b_M (i^* - \hat{d}_a + d) \quad (24b)$$

$$\epsilon \dot{\eta}_1 = -k_1 \eta_1 \quad (24c)$$

$$\epsilon \dot{\eta}_2 = -k_2 \eta_2 + b_M \hat{d}_a + \delta \quad (24d)$$

$$\epsilon \dot{\hat{d}}_a = -\frac{k_3}{\hat{b}_M} \eta_2. \quad (24e)$$

To find the quasi-steady-state solution of (24), stability of the boundary-layer system should be checked. To this end, the characteristic equation of the boundary-layer system (24c)–(24e) is earned

$$(s + k_1) \left(s^2 + k_2 s + \frac{b_M}{\hat{b}_M} k_3 \right) = 0, \quad (25)$$

implying to the fact that if $b_M/\hat{b}_M > 0$, (25) is Hurwitz because $k_i > 0$ ($i = 1, 2, 3$).

When (25) is Hurwitz and $\epsilon \ll 1$, according to the singular perturbation analysis, the quasi-steady-state solution satisfies the following property.

$$\eta_1 = \eta_2 = 0 \quad \text{and} \quad b_M \hat{d}_a = -\delta. \quad (26)$$

Substitution of the property in (24b) enables to derive the quasi-steady-state system version of (24):

$$\dot{x}_1 = x_2 \quad (27a)$$

$$\dot{x}_2 = \hat{a}_M x_1 - \hat{b}_M i^*. \quad (27b)$$

Hence, it can be said that the system of (17)–(18) behaves like the nominal system as $\epsilon \rightarrow 0$ under the stability condition of (25). (The performance analysis on the feedforward compensation by PIO_b can be similarly done.)

Remark 1 When only the position information is available for the outer-loop PIO_a , the output matrix reduces to $C_a = [1 \ 0 \ 0]$. Using the observer gain

$$L_a = [k_1/\epsilon, \quad \hat{a}_M + k_2/\epsilon^2, \quad -k_3/(\hat{b}_M \epsilon^3)]^T, \quad (28)$$

one can obtain the same performance recovery property if the next equation is Hurwitz.

$$s^3 + k_1 s^2 + k_2 s + \frac{b_M}{\hat{b}_M} k_3 = 0. \quad (29)$$

Certainly, it can be made Hurwitz by adjusting the parameters based on the physical bound of b_M and the root locus method [18].

5 Simulation Results

The performance of the proposed controller, in the presence of system parameter uncertainties and external disturbances, has been verified by comparative computer simulations. In the simulations, the desired elevation, x_e , that needs to be tracked by the outer-loop controller is constantly 7 mm. And the corresponding current, i_e , that needs to be tracked by the inner-loop controller equals to 1 A. Thus, the simulations aim to prove that the proposed controller can maintain the desired operation values under such severe conditions. The initial values of the states variables $[x \ \dot{x} \ i]^T$ were chosen to be $[0.01 \ 0 \ 0]^T$. In order to reflect physical

constraints, the control input in the simulations was limited to 100V in magnitude.

5.1 Robustness Improvement

System parameter variations are introduced in a manner that can reflect component performance deterioration and other environmental influences such as temperature change. The nominal and actual values of the system parameters are specified in Table 1.

External disturbances are also inserted into both loops separately: two time-varying noise signals and one constant disturbance. The inner-loop disturbance added to the control input in the fashion of a varying noise consists of two different signals, of which one is a constant between 0.5 and 0.6 s, while the other is a random time-varying signal of unknown function. The outer-loop disturbance is designed to mimic a physical disturbance (a downward pull of 3 mm at $t = 1$ s) acting on the ball. Designing the external disturbance in that way allows to see how well both PIOs can estimate the disturbance in their respective loop. It also helps evaluate the effect a disturbance in one loop has on the performance of the other loop’s controller.

It has been mentioned previously that one of the advantages of cascade configuration is its ability to be implemented on control systems that can be decoupled during design. This allows the option of integrating only one of the control loops with a PIO. In this context, The first is designed with a PIO only in the outer-loop (Controller 1 in Table 2 and the blue dotted line in Fig. 6), the second with a PIO only in the inner loop (Controller 2 in Table 2 and the red dashed line in Fig. 6), and finally the third with a PIO in each loop (Controller 3 in Table 2 and the black solid line in Fig. 6). The original control scheme discussed in Sect. 2 is referred to as Controller 0 in Table 2.

The controller’s performance is evaluated in terms of its ability to track the reference ball position in the presence of system parameter uncertainty, to recover from external disturbance, and to estimate the equivalent disturbances. As follows are the simulation results.

From the ball position simulation result in Fig. 6, it can be seen that the controller integrated with dual PIOs (black line) performs best out of the three non-nominal cases. It recovers fastest from disturbances (seen in the steady state

Table 1 System parameter values

Parameter	Nominal	Actual	Unit
m	0.068	0.125	kg
R	11	17	Ω
L	0.45	0.75	H
G_i	$3.2654e-5$	$2.99e-5$	Nm^2/A^2

Table 2 Control schemes considered

Controller	Inner PI	Inner PIO	Outer PI	Outer PIO
Controller 0	O	X	O	X
Controller 1	O	X	O	O
Controller 2	O	O	O	X
Controller 3	O	O	O	O

performance), resists the effect of system parameter uncertainties (seen in the transient state performance), and tracks the reference signal most accurately. Therefore, in view of this controller’s ability to closely approximate the nominal performance (green line), it is proposed as a robust controller for maglev systems. It can also be discovered in Fig. 7 that the proposed controller applies control input of appropriate magnitude to the system faster than the other two versions.

5.2 Disturbance Estimation

The simulations also reveal that the performance of the controller depends on its ability to access to an estimated disturbance. See Figs. 8 and 9. The controller equipped only with PIO_b (red dashed line in Fig. 6) fails to compensate for the effect of the outer-loop disturbance. Hence it is unable to quickly recover from it as shown in the figure. Meanwhile, the controller only with PIO_a (blue dotted line in Fig. 6) cannot counteract the effect of the inner-loop disturbance (as can be seen from its performance between 0.5 and 0.6 s). But it rapidly recovers from the outer-loop disturbance showing a good steady-state performance. It is owing to the inner-loop PI controller’s ability to ensure zero steady-state error.

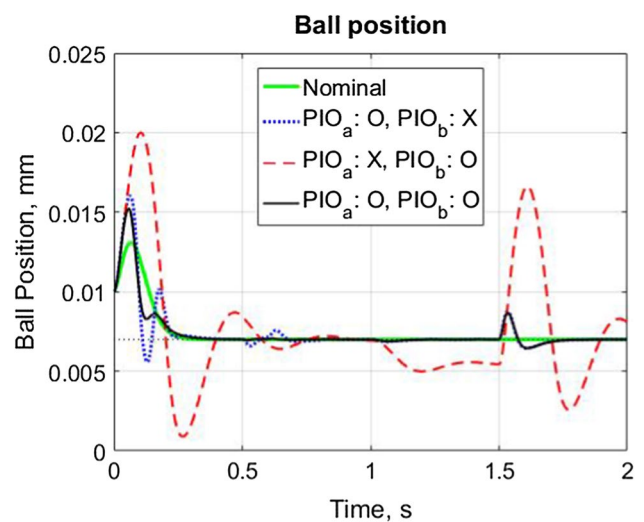


Fig. 6 Simulation result showing the performances of the three versions of the PIO-based controller

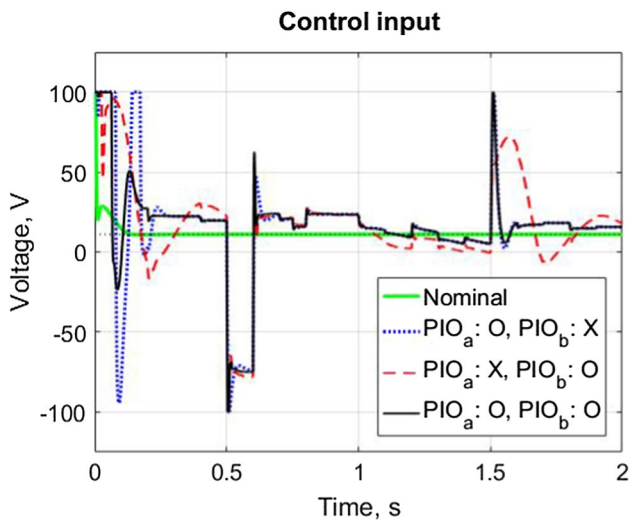


Fig. 7 Control input

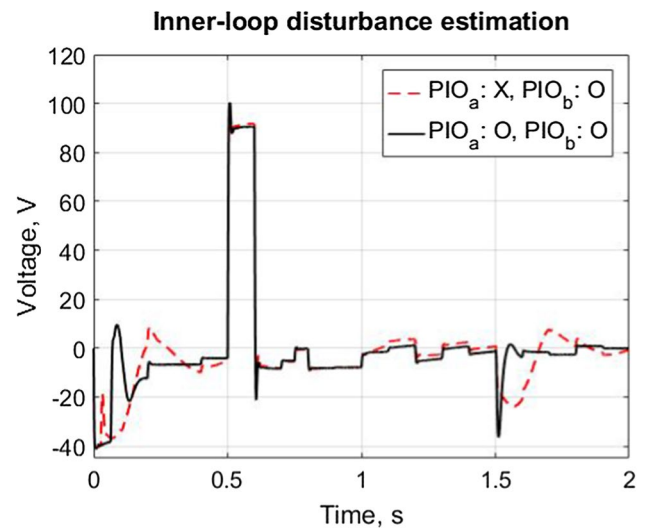


Fig. 9 Estimated equivalent disturbance in the inner loop

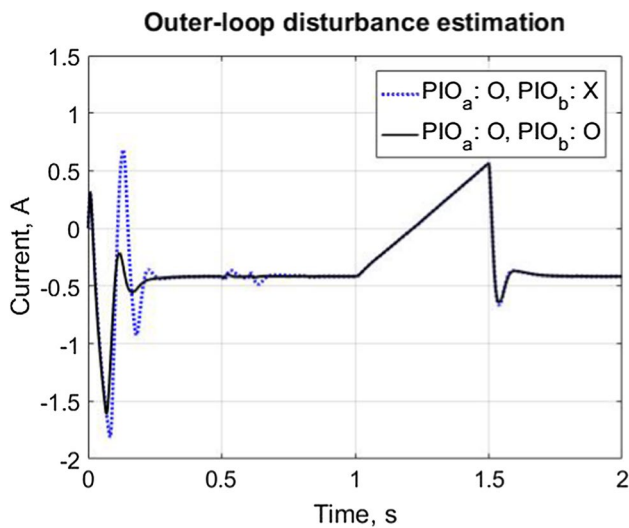


Fig. 8 Estimated equivalent disturbance in the outer loop

This means that when integrating a PIO with a cascade configuration controller, all the loops need to have individual PIOs to guarantee that the nominal performance of each control loop is well maintained. It is noteworthy that the performance of the observer in Figs. 8 and 9 can be further enhanced by performing multiple integrations of the estimation error and the measurement output simultaneously [19, 30].

The controller and observer gains were obtained by pole placement techniques. The poles were chosen following the rule of cascade control. The inner-loop system, which is an electrical system, is much faster than the electromechanical outer-loop system. Therefore, since the inner-loop controller and observer are expected to be faster than their outer-loop counterparts, the poles of the inner-loop controller and

observer are placed further away from the imaginary axis than those of outer-loop controller and observer. Similarly, since the observer in each loop is expected to be significantly faster than the controller, the locations of the observer poles are chosen further away leftward from the controller poles.

The outer-loop controller gains result from placing the closed-loop poles at $-20 \pm j10$ and -50 . They are

$$k_{p1} = -270.41, k_{p2} = -4.59, k_{I1} = -1275.50. \quad (30)$$

And the outer-loop PIO poles are placed at $-250, -250$ and -275 to obtain the observer gains:

$$L_a = \begin{bmatrix} 2.50 \times 10^2 & 1 \\ 2.80 \times 10^3 & 5.25 \times 10^2 \\ 0 & -3.51 \times 10^3 \end{bmatrix}. \quad (31)$$

For the inner-loop, controller gains are obtained as follows by placing the two closed-loop poles equally at -300 .

$$k_{p3} = 2.59 \times 10^2, k_{I2} = 4.05 \times 10^4. \quad (32)$$

And the PIO poles are placed equally again at -1250 , resulting in an observer gain matrix

$$L_b = \begin{bmatrix} 2.48 \times 10^3 \\ 7.03 \times 10^5 \end{bmatrix}. \quad (33)$$

The overall improvement made on the result of the existing control scheme can be observed in Figs. 10 and 11. They are summarized as follows.

1. Improved transient response in view of the overshoot and the settling time. The original controller's settling time 0.86 has reduced to 0.37 s.

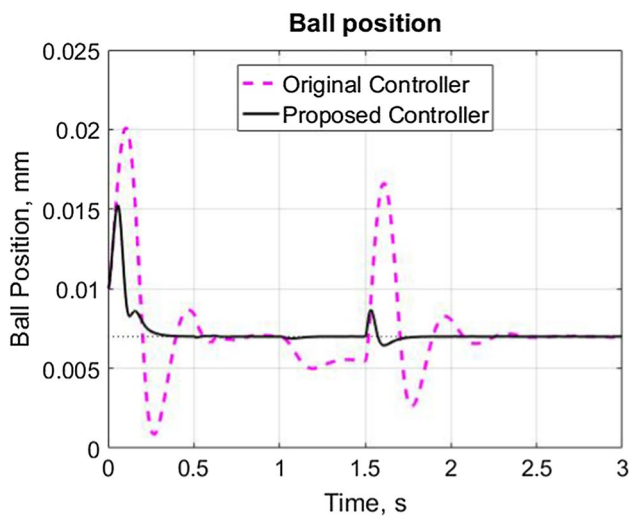


Fig. 10 Control performance improvement in ball position

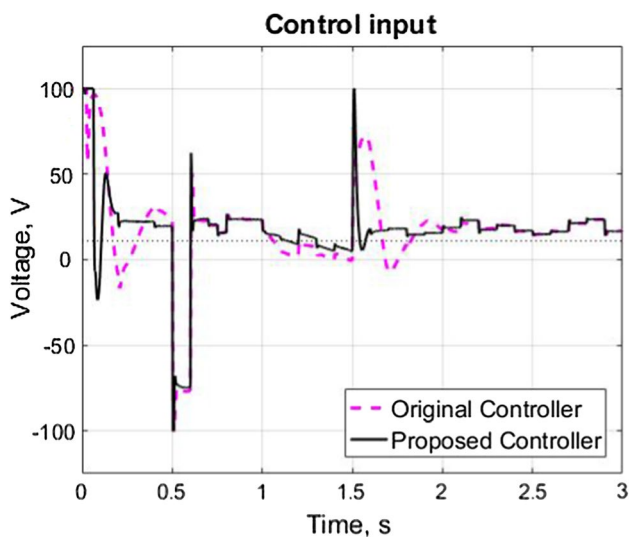


Fig. 11 Control performance improvement in control input

2. Stronger resistance to external disturbance and faster recovery as seen from $t = 1$ to 2 s.
3. Smaller control input as seen in Fig. 11.

6 Conclusion

Maglev systems belong to a class of systems that are challenging but at the same time implemented in delicate applications where reliable control systems are in demand. Moreover, the existence of system parameter uncertainties and external disturbances makes the challenge even greater.

In this context, this paper has proposed a robust controller that can overcome those negative influences for a single-axis

magnetic levitation system. The new control system has been designed by cascading two PI controllers each with a nested PIO. The design procedure was detailed and theoretical analysis was carried out according to the singular perturbation theory to verify that the resultant integrated system can approximate the nominal system even under severe conditions.

The performance of the proposed controller was also tested by simulations and its ability to robustly maintain nominal performance was proved. It has also been confirmed from the simulation results that optimum system performance is guaranteed only when every control loop is unexceptionally integrated with a PIO. However, if the control loop that is highly vulnerable to parameter uncertainty and disturbance can be identified and if those in the other loop are negligible, then the results may indicate that adequate performance can be obtained even when a PIO is included only in the former control loop. Since the system under consideration in this paper is a single axis magnetic levitation system, the future work aims at tackling a more practical, and yet complex magnetic levitation system with more degrees of motional freedom.

Acknowledgements The authors would like to thank the anonymous reviewers for their valuable comments that helped to improve this paper.

References

1. Hajjaji AE, Ouladsine M (2001) Modeling and nonlinear control of magnetic levitation system. *IEEE Trans Ind Electron* 48(4):831–838
2. Bushway RR (2001) Electromagnetic aircraft launch system development considerations. *IEEE Trans Magn* 37(1):52–54
3. Lee HW, Kim KC, Lee J (2006) Review of maglev train technologies. *IEEE Trans Magn* 42(7):1917–1925
4. Kim WJ, Verma S, Shakir H (2007) Design and precision construction of novel magnetic-levitation-based multi-axis nanoscale positioning systems. *Precis Eng* 31:337–350
5. Bidikli B, Bayrak A (2018) A self-tuning robust full-state feedback control design for the magnetic levitation system. *Control Eng Pract* 78:175–185
6. Bonivento C, Gentili L, Marconi L (2005) Balanced robust regulation of a magnetic levitation system. *IEEE Trans Control Syst Technol* 13(6):1036–1044
7. Yang ZJ, Kunitoshi K, Kanae S, Wada K (2008) Adaptive robust output-feedback control of a magnetic levitation system by K-filter approach. *IEEE Trans Ind Electron* 55(1):390–399
8. Gluck T, Kemmetmuller W, Tump C, Kugi A (2011) A novel robust position estimator for self-sensing magnetic levitation systems based on least squares identification. *Control Eng Pract* 19(2):146–157
9. Bachle T, Hentzelt S, Graichen K (2013) Nonlinear model predictive control of a magnetic levitation system. *Control Eng Pract* 21(9):1250–1258
10. Ghosh A, Krishnan TR, Tejaswy P, Mandal A, Pradhan JK, Ranasingh S (2014) Design and implementation of a 2-DOF

- PID compensation for magnetic levitation systems. *ISA Trans* 53(4):1216–1222
11. de Jesús Rubio J, Zhang L, Lughofer E, Cruz P, Alsaedi A, Hayat T (2017) Modeling and control with neural networks for a magnetic levitation system. *Neurocomputing* 227:113–121
 12. Starbino AV, Sathiyavathi S (2019) Design of sliding mode controller for magnetic levitation system. *Comput Electr Eng* 78:184–203
 13. Wei W, Xue W, Li D (2019) On disturbance rejection in magnetic levitation. *Control Eng Pract* 82:24–35
 14. Campos-Rodríguez A, García-Sandoval JP, González-Álvarez V, González-Álvarez A (2019) Hybrid cascade control for class of nonlinear dynamical systems. *J Process Control* 76:141–154
 15. Errouissi R, Al-Durra A, Mueeen SM (2018) Experimental validation of a novel PI speed controller for AC motor drives with improved transient performances. *IEEE Trans Control Syst Technol* 26(4):1414–1424
 16. Selvaraj P, Sakthivel R, Anthoni SM, Rathika M, Mo YC (2016) Dissipative sampled-data control of uncertain nonlinear systems with time-varying delays. *Complexity* 21:142–154
 17. Choi Y, Yang K, Chung WK, Kim HR, Suh IH (2003) On the robustness and performance of disturbance observers for second-order systems. *IEEE Trans Autom Control* 48(2):315–320
 18. Back J, Shim H (2008) Adding robustness to nominal output-feedback controllers for uncertain nonlinear systems: a nonlinear version of disturbance observer. *Automatica* 44:2528–2537
 19. Kim KS, Rew KH, Kim S (2010) Disturbance observer for estimating higher order disturbances in time series expansion. *IEEE Trans Autom Control* 55(8):1905–1911
 20. Chen WH, Yang J, Guo L, Li S (2016) Disturbance-observer-based control and related methods—an overview. *IEEE Trans Ind Electr* 63(2):1083–1095
 21. Shim H, Park G, Joo Y, Back J, Jo NH (2016) Yet another tutorial on disturbance observer: robust stabilization and recovery of nominal performance. *Control Theory Technol* 14(3):237–249
 22. Yook JH, Kim IH, Han MS, Son YI (2017) Robustness improvement of DC motor speed control using communication disturbance observer under uncertain time delay. *Electron Lett* 53(6):389–391
 23. Jo NH, Jeon C, Shim H (2017) Noise reduction disturbance observer for disturbance attenuation and noise suppression. *IEEE Trans Ind Electron* 64(2):1381–1391
 24. Sakthivel R, Raajananthini K, Selvaraj P, Ren Y (2018) Design and analysis for uncertain repetitive control systems with unknown disturbances. *J Dyn Syst Meas Control* 140(12):121007. <https://doi.org/10.1115/1.4040663>
 25. Sariyildiz E, Oboe R, Ohnishi K (2020) Disturbance observer-based robust control and its applications: 35th anniversary overview. *IEEE Trans Ind Electron* 67(3):2042–2053
 26. Beale SR, Shafai B (1989) Robust control system design with a proportional integral observer. *Int J Control* 50(1):97–111
 27. Kim IH, Son YI (2017) A modular disturbance observer-based cascade controller for robust speed regulation of PMSM. *J Electr Eng Technol* 12(4):1663–1674
 28. Khalil HK (1996) *Nonlinear systems*, 2nd edn. Prentice-Hall, Upper Saddle River
 29. Quanser Inc. (2008) *Magnetic levitation experiment (user manuals)*

30. Son YI, Kim IH (2010) A robust state observer using multiple integrators for multivariable LTI systems. *IEICE Trans Fundam Electron Commun Comput Sci* E93–A(5):981–984

Publisher's Note Springer Nature remains neutral with regard to jurisdictional claims in published maps and institutional affiliations.



Amare Nebiyeleul Daniel received his B.S. degree from Addis Ababa Science and Technology University, Ethiopia, in 2017. He is currently working towards his M.S. degree at Myongji University, Korea. His current research interests are robust control and industrial applications using artificial intelligence.



Young Ik Son received the B.S., M.S., and Ph.D. degrees from Seoul National University, Korea, in 1995, 1997 and 2002, respectively. He was a visiting scholar at Cornell University (2007–2008) and University of Connecticut (2016–2017). Since 2003, he has been with the Department of Electrical Engineering at Myongji University, Korea, where he is currently a professor. His research interests include robust controller design and its application to industrial electronics.



Seungchul Lim received the B.S., M.S., and Ph.D. degrees from Seoul National University, KAIST, and Virginia Tech in 1981, 1983 and 1992 respectively. He is currently with ME department of Myongji University as a professor. His research interests include robotics and design of high-performance dynamic systems.